

## Isothermal and Non-Isothermal Flow of PTT Fluid in Lid-Driven Polar Cavity

Hatice Mercan, Kunt Atalık

Mechanical Eng. Dep., Boğaziçi University, 34342 Bebek, Istanbul, Turkey

### ABSTRACT

In this study isothermal and non-isothermal viscoelastic PTT fluid flow in a lid driven polar cavity is considered. The effects of elasticity and viscous heating on the flow and stress fields are demonstrated and compared in terms of vortical structure, stress components and temperature distributions in the polar cavity.

### INTRODUCTION

The purpose of this study is to analyse the viscoelastic and non-isothermal effects with viscous dissipation for two dimensional flow in a polar cavity. The flow is induced by the motion of the inner curved wall. The polar cavity geometry can be considered as a typical cross section of a single screw extruder<sup>1</sup>, and is suitable to illustrate the effect of curved geometry on an internal viscoelastic flow field. This geometry (with cavity angle of 1 radian and gap ratio of  $\frac{1}{2}$ ) is first used and described in a study by Fuchs and Tillmark<sup>2</sup>, where they obtained numerical simulation results for Newtonian case at considerably low Reynolds numbers. Wu et al.<sup>3</sup> solved for polar cavity flow of a Newtonian fluid up to Reynolds number 1000 and used this case as a validation tool for their new Lagrange interpolation method. Lei et al.<sup>4</sup>, Darbandi and Vakili-pour<sup>5</sup> and Kim<sup>6</sup> used the same geometry as a test case to validate their

numerical schemes. Krasnopolskaya<sup>1</sup> used this geometry (with a cavity angle of  $\pi/2$ ), to model mixing in a single screw extruder.

The effects of viscous dissipation on Newtonian and non-Newtonian flow fields have been studied by many researchers, for similar geometries. Al-Mubaiyedh et al.<sup>7</sup> investigated the influence of viscous heating on the stability of Taylor-Couette flow for Newtonian fluids with thermally sensitive viscosity. Basing on the linear stability analysis, they showed that viscous heating leads to significant destabilization in Taylor Couette flow. Yeşilata<sup>8</sup> investigated how to predict the material properties of viscoelastic fluids under viscous dissipation effects. He formulated the problem for the flow of an Oldroyd B fluid between two rotating parallel plates. Yataghene et al.<sup>9</sup> analysed both experimentally and numerically the increase of temperature due to viscous dissipation for Newtonian and non-Newtonian power-law (shear thinning) fluids for the flow in a scraped surface heat exchanger. They remarked an increase in viscous heating as the rotor speed increases. However, they reported that the effect of viscous dissipation was not observed for the power-law fluid. They attributed this behaviour to the shear thinning character of the fluid which considerably reduces the apparent viscosity and therefore the viscous dissipation in the high shear rate zones near the blade.

In this study we investigate the non-isothermal and viscoelastic flow of a Phan-Thien-Tanner (PTT) fluid in a lid driven  $\pi/2$  angle polar cavity with a gap ratio  $h=4/7$ . As a general model Williams-Landel-Ferry equation is used to describe the temperature dependence of the material parameters such as viscosity and relaxation time.

The viscous dissipation effect on the flow field is shown and compared for Newtonian and viscoelastic cases. The results are presented in terms of streamlines, isotherms and centreline velocity components and temperature distributions.

#### FORMULATION AND METHOD OF SOLUTION

We consider the 2-D flow of a polymer solution in a polar cavity with cavity angle  $\theta_p=\pi/2$  and gap ratio (ratio of inner radius  $r_i$  to outer radius  $r_o$ ) of  $h=4/7$  (Fig. 1). The outer wall and the side walls are fixed, while the inner lid moves in  $\theta$  direction with a predefined velocity distribution. The fluid is initially at rest and we specify no-slip boundary conditions at the walls. The  $\theta$  component of the moving inner lid velocity is given by,

$$U_i(t, \theta) = \frac{8}{(\pi/2)^4} [1 + \tanh 8t - 4] \left(\frac{\pi}{4} - \theta\right)^2 \left(\frac{\pi}{4} + \theta\right)^2 \quad (1)$$

where  $t$  denotes the time. This new definition of the distributed lid velocity, inspired from a study by Fattal and Kupferman<sup>10</sup>, helps to prevent the singularities at cavity corners without causing any significant qualitative and quantitative change on the vortical structure compared to constant lid velocity case as shown in (Fig.2 (a) and (b)). The  $r$  component of the velocity vanishes at the walls. The outer wall is kept at constant high temperature  $T_o$ , while the moving inner lid is kept at constant low temperature  $T_i$  ( $T_o > T_i$ ). The stationary side walls are insulated.

Since this geometry is a better approximation in two dimensional space for the single screw extruders compared to the rectangular cavity, the thermal boundary conditions are determined according to this application<sup>12</sup>.

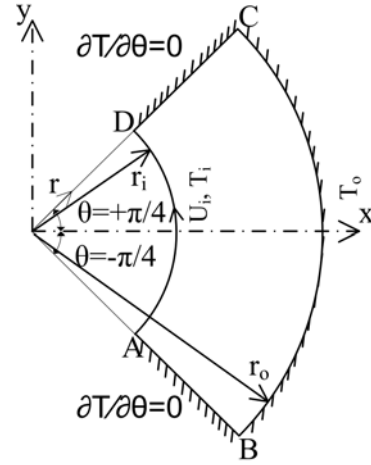


Figure 1. Cavity Geometry

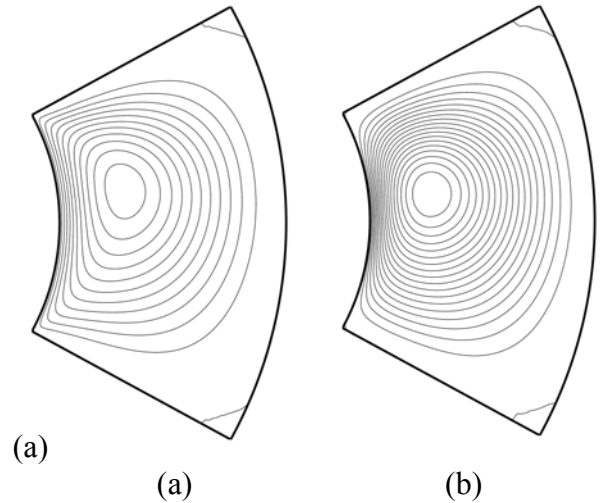


Figure 2. Newtonian polar cavity flow ( $\theta_p=\pi/2$ ,  $h=1/2$ ) at  $Re=60$  (a) constant lid velocity case,  $\Psi_{min}=-0.116336$  (b) distributed lid velocity case,  $\Psi_{min}=-0.1094$

The conservation equations for non-isothermal, incompressible viscoelastic flow can be written in dimensionless form as,

$$\nabla \cdot \underline{V} = 0 \quad (2)$$

$$\text{Re} \frac{D\underline{V}}{Dt} = -\nabla p + \beta(T)\nabla^2 \underline{V} + (1 - \beta(T))\nabla \cdot \underline{T} \quad (3)$$

$$\frac{DT}{Dt} = \frac{1}{Pe}(\nabla^2 T + Br(\alpha(\underline{T} : \underline{D}) + (1 - \alpha)\frac{\text{tr}(\underline{T})}{2We(T)})) \quad (4)$$

where  $\underline{V}$  is the velocity vector,  $\underline{T}$  is the viscoelastic extra-stress tensor,  $p$  is pressure  $T$  is temperature and  $D/Dt$  denotes the material derivative. The Reynolds number is defined as  $\text{Re} = \rho V_0 r_i / \mu$ , where  $\rho$  is the fluid density,  $V_0$  is the characteristic velocity and  $\mu$  is the total shear rate viscosity. In this study we used low ( $\text{Re}=0.3$ , in viscoelastic cases) to moderate ( $\text{Re}=60$ , in Newtonian cases) Reynolds numbers. The dimensionless parameter  $\beta$  is the ratio of the solvent viscosity ( $\mu_s$ ) to the total zero-shear rate viscosity ( $\mu = \mu_s + \mu_p$ , with  $\mu_p$ , the polymer viscosity) and has been fixed as  $\beta=0.45$  in this study. Péclet number is defined as  $Pe = \rho C_p V_0 r_i / k$ , where  $C_p$  is the heat capacity and  $k$  is the thermal conductivity, and has been chosen as  $Pe=500$  and  $Pe=900$ . Brinkman number represents the ratio of viscous dissipation to heat conduction resulting from imposed temperature difference, which signifies self heating versus external heating, and is defined as  $Br = \frac{\mu V_0^2}{k(T_w - T_0)}$ . In this study it

is fixed to the value of  $Br=15$ . The dissipation term in the energy equation (4) is composed of two parts, namely, viscous dissipation and elastic dissipation. More precisely,  $\alpha=0$  is the pure elastic dissipation case and  $\alpha=1$  is the pure viscous dissipation case. The non-dimensional temperature is

defined as  $T = \frac{\tilde{T} - T_i}{T_o - T_i}$  where  $\tilde{T}$  is the dimensional temperature. Weissenberg number is defined as  $We = \lambda V_0 / r_i$ , where  $\lambda$  is the relaxation time of the fluid.

In this study the temperature difference ( $T_o - T_i$ ) is considered at the order of  $1^\circ\text{K}$ , hence the fluid can be assumed incompressible<sup>7</sup>. The density and thermal conductivity are assumed independent of temperature field. However polymer viscosity and relaxation time of the polymer additive are assumed to be temperature dependent. The temperature dependence of the non-dimensional Weissenberg number and viscosity ratio are as follows

$$We(T) = We f(T) \quad (5)$$

$$\beta(T) = 1 - \omega_r f(T)$$

where  $\omega_r$  is the retardation parameter defined as the ratio of  $\frac{\mu_p}{\mu}$  and the temperature dependency function,  $f(T)$ , is defined according to Williams-Landel-Ferry (WLF) model which reads;

$$f(T) = \exp\left[-\frac{c_1 T}{c_2(T_o - T_i) + T}\right] \quad (6)$$

We set the quantities  $T_o - T_i = 1$ ,  $c_1=15$  and  $c_2=50$  following the literature<sup>11</sup>.

In this study Phan-Thien-Tanner constitutive relation is used to model the viscoelastic fluid. In dimensionless form the Phan-Thien-Tanner model reads,

$$\underline{T} + We(T)(\overset{\nabla}{T} + \text{tr}(\underline{T})\underline{T}) = 2\underline{D} \quad (7)$$

where  $\underline{D}$  is the rate of deformation tensor and the operator  $\overset{\nabla}{( )}$  denotes the upper convected derivative as follows,

$$\underline{\underline{T}} = \frac{D\underline{\underline{T}}}{Dt} - \underline{\underline{L}} \cdot \underline{\underline{T}} + \underline{\underline{T}} \cdot \underline{\underline{L}} \quad (8)$$

where  $\underline{\underline{L}}$  is the velocity gradient.

The stream function-vorticity formulation in cylindrical coordinates is adopted and the governing equations are solved numerically using a second order centred finite difference scheme. The explicit Runge-Kutta-Fehlberg method with time step adjustment is used for time integration and parameter continuation technique is applied. Elliptic stream function-vorticity equation is solved by successive over relaxation (SOR) method with Chebychev acceleration. The grid independency test results are shown in Fig. 3 for different grid densities and a structured grid with (65x49) grid density is chosen for simulations.

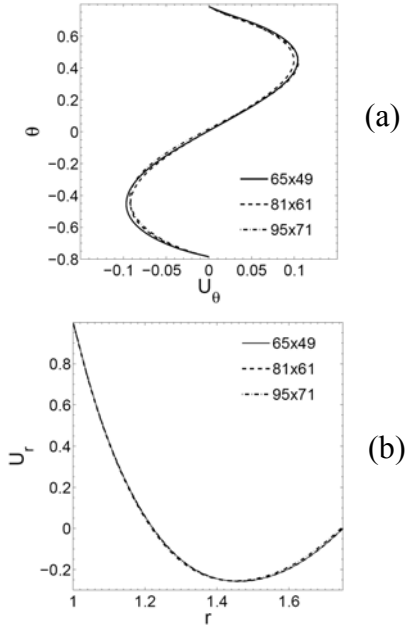


Figure 3. Velocity component profile comparison along the centreline at  $Re=3$ ,  $We=0.25$ ,  $\beta=0.75$ ,  $Pe=60$ ,  $\alpha=0.5$  and  $Br=0.25$  for various grid densities (a) transverse velocity component (b) radial velocity component

## RESULTS AND DISCUSSION

We present first the dissipation effect for a Newtonian fluid at moderate Reynolds

number. Then elastic effects are shown by comparing non-isothermal Newtonian and PTT fluid flows. The thermal effects on the stress field are also demonstrated.

### The effect of viscous dissipation in Newtonian flow:

We first investigate the effects of viscous dissipation in the Newtonian case. In Fig. (4) the streamlines are shown for isothermal and non-isothermal Newtonian flow at  $Re=60$ ,  $Pe=500$ ,  $Br=15$ . The central vortex is observed to shift in the positive  $\theta$  direction under viscous dissipation. The maximum and minimum stream function values are also given with peak locations.

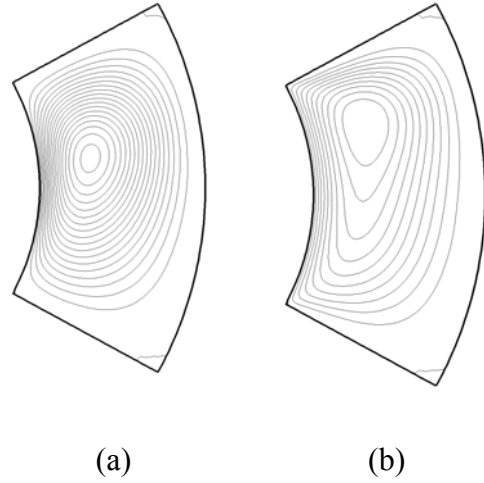


Figure 4. Streamlines for Newtonian flow at  $Re=60$  (a) Isothermal case  $\Psi_{min}=-0.09232, \Psi_{max}=0.0000064, x_{min}=1.2274, y_{min}=0.1352$ , (b) Non-Isothermal case ( $Pe=500, Br=15$ )  $\Psi_{min}=-0.111656, \Psi_{max}=0.00002092, x_{min}=1.2248, y_{min}=0.3125$

In Fig. (5) radial velocity component profile is plotted along  $r=1.23$  line where the minimum stream function and maximum temperature peaks are located. An increase in the peak value of the radial velocity component is observed in the non-isothermal case. The isotherms can be observed in Fig. (6), where the viscous heating increases appreciably reaching  $T \approx 1.84$ . The maximum and peak values of

the temperature coincide and the viscous heating is observed to occur in the upper left part of the cavity. In this Newtonian case as the Reynolds number is moderate; the viscous heating is pronounced.

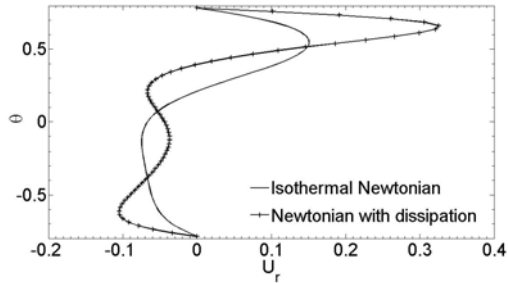


Figure 5 Radial velocity component profiles along  $r=1.23$  at  $Re=60$  for Newtonian isothermal and non-isothermal cases ( $Pe=500, Br=15$ )

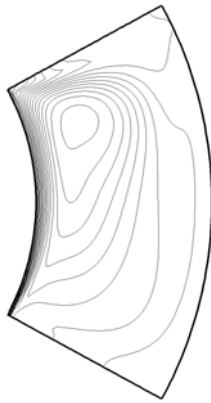


Figure 6. Isotherms for Newtonian flow at  $Re=60, Pe=500, Br=15, T_{max}=T_{peak}=1.83998, T_{min}=0, x_{max}=1.1845, y_{max}=0.3436$

The effects of elasticity under thermal dissipation:

In this case the effects of elasticity are investigated by comparing the non-isothermal Newtonian case and non-isothermal viscoelastic PTT case. In Fig. (7) the streamlines for  $Re=0.3$  are plotted. The vortical structure displays a longitudinal elongation in transverse direction with viscous dissipation at this low Reynolds number for Newtonian case (Fig. (7a)) compared to viscoelastic case with  $We=1, \beta=0.45$  (Fig. (7b)). Also the upper right

corner vortex is observed to disappear under elastic effects.

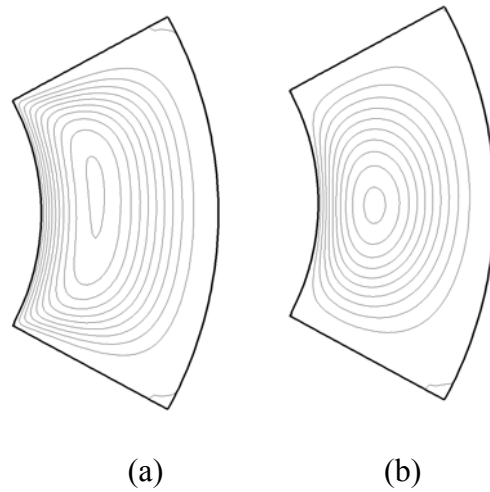


Figure 7. Streamlines for  $Re=0.3, Pe=900, Br=15$  (a) Newtonian,  $\Psi_{min}=-0.101621, \Psi_{max}=0.00001072, x_{min}=1.2285, y_{min}=0.12312$  (b) Non-Newtonian PTT model,  $We=1.0, \beta=0.45, \alpha=0.5, \Psi_{min}=-0.102764, \Psi_{max}=0.000000375, x_{min}=1.235, y_{min}=-0.00881$

The isotherms are shown in Fig. (8). Although the viscous heating is present in the Newtonian case it is not observed in viscoelastic case. The location is shifting to the center and its value is decreasing as shown in Fig. (8(a-b)). In Fig. (9) the centreline temperature profiles are given for various  $\alpha$  values at  $\theta=0$ . In Fig. (10) the centreline radial velocity component is displayed for both cases. It is observed that the temperature peak values are increased in the pure viscous dissipation ( $\alpha=1.0$ ) and the pure elastic dissipation cases ( $\alpha=0.0$ ) compared to  $\alpha=0.5$  case.

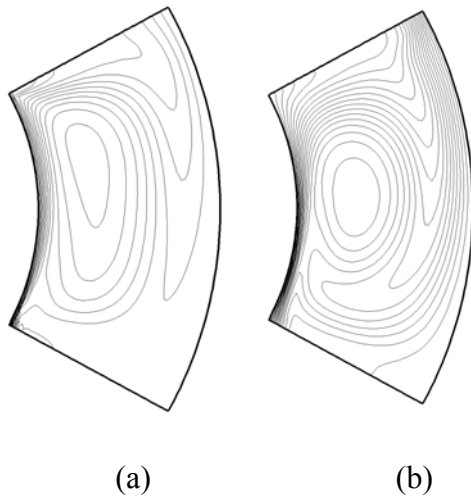


Figure 8. Isotherms for  $Re=0.3$ ,  $Pe=900$ ,  $Br=15$ , (a) Newtonian,  $T_{max}=T_{peak}=1.44799$ ,  $x_{max}=1.1996$ ,  $y_{max}=0.216$  (b) PTT,  $We=1.0$ ,  $\beta=0.45$ ,  $\alpha=1.0$ ,  $T_{max}=1$ ,  $T_{min}=0$ ,  $T_{peak}=0.9465$ ,  $x_{peak}=1.2491$ ,  $y_{peak}=0.0239$

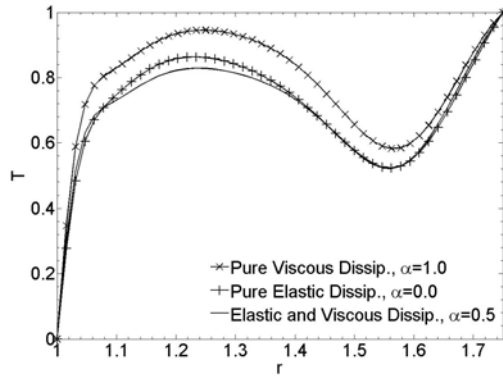


Figure 9 Temperature profiles for PTT case along the centerline  $\theta=0$  at  $Re=0.3$ ,  $Pe=900$ ,  $Br=15$ ,  $We=1.0$ ,  $\beta=0.45$ , for different  $\alpha$  values.

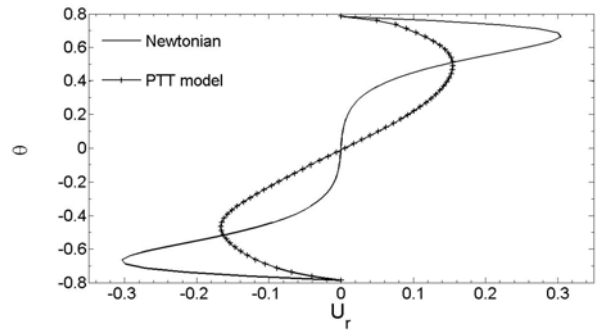


Figure 10 Radial velocity component profiles along  $r=1.23$  at  $Re=0.3$  for non-isothermal Newtonian and viscoelastic PTT cases ( $We=1.0$ ,  $\beta=0.45$ ,  $\alpha=1.0$ )

The isothermal PTT flow and non-isothermal PTT flow are compared in terms of stress distributions. In Fig. (11) the normal stress difference along the  $r=1.23$  is shown, and in Fig. (12) the centreline shear stress distribution along the  $\theta=0$  is shown. In both cases the peak values in the stresses are increased.

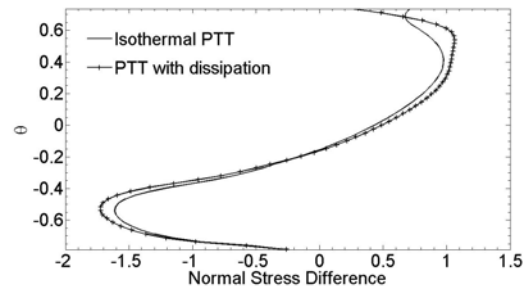


Figure 11 First normal stress difference profiles  $r=1.23$  at  $Re=0.3$ ,  $We=1.0$ ,  $\beta=0.45$ , for isothermal and viscoelastic PTT cases ( $Pe=900$ ,  $Br=15$ ,  $\alpha=0.5$ ).

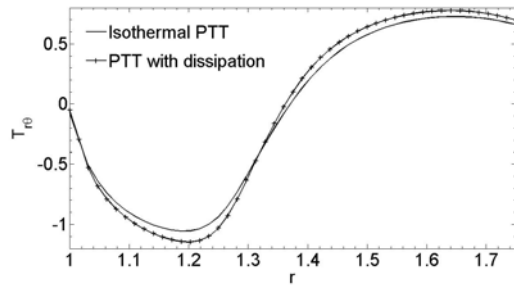


Figure. 12 Shear stress profiles along the centreline  $\theta=0$  at  $Re=0.3$ ,  $We=1.0$ ,  $\beta=0.45$  for isothermal and non-isothermal viscoelastic PTT cases ( $Pe=900$ ,  $Br=15$ ,  $\alpha=0.5$ )

## CONCLUSION

Isothermal and non-isothermal flows of a viscoelastic fluid have been studied numerically for the lid-driven polar cavity geometry with cavity angle of  $\theta_p=\pi/2$  and gap ratio of  $h=4/7$ . The results have been compared to Newtonian case.

In the Newtonian case the central vortex is observed to shift in the positive transverse direction and the peak value of the radial velocity component increases under viscous dissipation effects. The viscous heating occurs at the upper left part of the cavity.

The upper right corner vortex vanishes when elastic effects are present for low Reynolds number case ( $Re=0.3$ ) under thermal dissipation. Viscous heating is not observed in the viscoelastic case ( $We=1.0$ ,  $Pe=900$ ,  $Br=15$ ,  $\beta=0.45$ ). This can be explained by the decrease in apparent viscosity under shear thinning leading to a decrease in viscous dissipation. The peak location for the temperature distribution moves to the centre of the cavity and the value of this peak decreases under elastic effects. The peak value of the radial velocity component decreases as well. For viscoelastic non-isothermal case, the pure viscous dissipation case ( $\alpha=1.0$ ) leads to the highest peak of the temperature at the centreline and the pure elastic dissipation ( $\alpha=0.0$ ) leads to a lower peak, however in

both cases the temperature peaks are higher than  $\alpha=0.5$  case.

It is also observed that normal stress difference and shear stress peak values are increased under thermal dissipation for the viscoelastic case.

## ACKNOWLEDGMENTS

This work is supported by Boğaziçi University Scientific Research Projects (BAP) with project code 08A604.

## REFERENCES

1. Krasnopolskaya, T.S., Malshko V.V., Peters G.M.W., Meijer H.E.H., (1999), "Mixing in Stokes Flow in an Annular Wedge Cavity", *European Journal of Mechanics B/Fluids*, **18**, 793-822.
2. Fuchs, L. and Tillmark N., (1985), "Numerical and Experimental Study of Driven Flow in Polar Cavity", *International Journal of Numerical Methods in Fluids*, **5**, 311-319.
3. Wu, Z.G., Zhang J.Z., Zhou J.J., Tao W.Q., (2007), "A Simple and Effective Method for Enhancing Iteration Convergence of Incompressible Fluid Flow and Heat Transfer Simulations: Lagrange Interpolation for Initial Field", *Numerical Heat Transfer Part B: Fundamentals*, **51**, 229-249
4. Lei, C., Cheng L., Kavanagh K., (2000), "A Finite Difference Solution of Shear Flow Over a Circular Cylinder", *Ocean Engineering*, **27**, 271-290.
5. Darbandi M., Vakilipour S., (2008), "Developing Implicit Pressure Weighted Up Winding Scheme to Calculate Steady and Unsteady Flows on Unstructured Grids", (2008), *International Journal for Numerical Methods in Fluids*, **56**, 115-141.
6. Kim, S.-W., (1989), "Control Volume Based Navier Stokes Equation Solver Valid

at all Flow Velocities”, *NASA Technical Memorandum*, ICOMP-89-5.

7. Al- Mubaiyedh U. A., Sureshkumar R. Khomami B. (2002), “The Effect of Eiscous Eeating on the Stability of Taylor-Couette flow”, *J Fluid Mech.*, **462**, 111-132

8. Yeşilata B., (2002), “Effect of Viscous Dissipation on Polymeric Flows Between Two Rotational Coaxial Parallel Discs”, *Int. Com. Heat and Mass Transfer*, **29**, 5, 589-600

9. Yataghene M., Fayolle F., Legrand J., (2009) “Experimental and Numerical Analysis of Heat Transfer Including Viscous Dissipation in a Scraped Surface Heat Exchanger”, *Chemical Engineering and Processing*, **48**, 1445-1456

10. Fattal R., Kupferman R., (2005), “Time-Dependent Simulation of Viscoelastic Flows at High Weissenberg Number Using the log-Conformation Representation”, *J. Non-Newtonian Fluid Mech.*, **126**, 23-37

11. Kunisch K., Marduel X., (2000), “Optimal Control of non-isothermal Viscoelastic Fluid Flow”, *J. Non-Newtonian Fluid Mech.*, **88**, 261-301.

12. Karwe M.W., Jaluria Y., (1990), “Numerical Simulation of Fluid Flow and Heat Transfer in a Single Screw Extruder for non-Newtonian Fluids”, *Numerical Heat Transfer*, Part A, 17, 167-190.